Precision Measurement of Cosmic-Ray Nitrogen and its Primary and Secondary Components with the Alpha Magnetic Spectrometer on the International Space Station

M. Aguilar,[27] L. Ali Cavasonza,[1] B. Alpat,[32] G. Ambrosi,[32] L. Arruda,[25] N. Attig,[22] S. Aupetit,[17] P. Azzarello,[16] A. Bachlechner,[1] F. Barao,[25] A. Barrau,[17] L. Barrin,[15] A. Bartoloni,[37] L. Basara,[35] S. Başeğmez-du Pree,[6,2] M. Battarbee,[44] R. Battiston,[35,36,a] U. Becker,[10] M. Behlmann,[10] B. Beischer,[1] J. Berdugo,[27] B. Bertucci,[32,33] K. F. Bindel,[23] V. Bindi,[20] W. de Boer,[23] K. Bollweg,[21] V. Bonnivard,[17] B. Borgia,[37,38] M. J. Boschini,[29] M. Bourquin,[16] E. F. Bueno,[39] J. Burger,[10] W. J. Burger,[35] X. D. Cai,[10] M. Capell,[10] S. Caroff,[3] J. Casaus,[27] G. Castellini,[14] F. Cervelli,[34] Y. H. Chang,[11] A. I. Chen,[10] G. M. Chen,[6] H. S. Chen,[6,7] Y. Chen,[16] L. Cheng,[40] H. Y. Chou,[11] E. Choumilov,[10] V. Choutko,[10] C. H. Chung,[1] C. Clark,[21] R. Clavero,[24] G. Coignet,[3] C. Consolandi,[20] A. Contin,[8,9] C. Corti,[20] W. Creus,[43] M. Crispoltoni,[32,33] Z. Cui,[40] K. Dadzie,[10] Y. M. Dai,[5] A. Datta,[20] C. Delgado,[27] S. Della Torre,[29] M. B. Demirköz,[2] L. Derome,[17] S. Di Falco,[34] F. Dimiccoli,[35,15] C. Díaz,[27] P. von Doetinchem,[20] F. Dong,[31] F. Donnini,[32,b] M. Duranti,[32] A. Egorov,[10] A. Eline,[10] T. Eronen,[44] J. Feng,[10] E. Fiandrini,[32,33] P. Fisher,[10] V. Formato,[32] Y. Galaktionov,[10] G. Gallucci,[34] R. J. García-López,[24] C. Gargiulo,[15] H. Gast,[1] I. Gebauer,[23] M. Gervasi,[29,30] A. Ghelfi,[17] F. Giovacchini,[27] D. M. Gómez-Coral,[28] J. Gong,[31] C. Goy,[3] V. Grabski,[28] D. Grandi,[29,30] M. Graziani,[23] K. H. Guo,[19] S. Haino,[43] K. C. Han,[26] Z. H. He,[19] M. Heil,[10] T. H. Hsieh,[10] H. Huang,[43,c] Z. C. Huang,[19] M. Incagli,[34] Yi Jia,[10] H. Jinchi,[26] K. Kanishev,[35,15] B. Khiali,[11,32,b] Th. Kirn,[1] C. Konak,[2] O. Kounina,[10] A. Kounine,[10] V. Koutsenko,[10] A. Kulemzin,[10] G. La Vacca,[29,30] E. Laudi,[15] G. Laurenti,[8] I. Lazzizzera,[35,36] A. Lebedev,[10] H. T. Lee,[42] S. C. Lee,[43] C. Leluc,[16] H. S. Li,[41] J. Q. Li,[31] Q. Li,[31] T. X. Li,[19] Z. H. Li,[6] Z. Y. Li,[43,d] C. H. Lin,[43] P. Lipari,[37] T. Lippert,[22] D. Liu,[11] Hu Liu,[10] Z. Liu,[16] V. D. Lordello,[39] S. Q. Lu,[43,d] Y. S. Lu,[6] K. Luebelsmeyer,[1] F. Luo,[40] J. Z. Luo,[31] S. S. Lyu,[19] F. Machate,[1] C. Mañá,[27] J. Marín,[27] T. Martin,[21] G. Martínez,[27] N. Masi,[8] D. Maurin,[17] A. Menchaca-Rocha,[28] Q. Meng,[31] V. M. Mikuni,[39] D. C. Mo,[19] P. Mott,[21] L. Mussolin,[32,33] T. Nelson,[20] J. Q. Ni,[19] N. Nikonov,[1] F. Nozzoli,[35] A. Oliva,[27] M. Orcinha,[25] M. Palermo,[20] F. Palmonari,[8,9] C. Palomares,[27] M. Paniccia,[16] M. Pauluzzi,[32,33] S. Pensotti,[29,30] C. Perrina,[16] H. D. Phan,[10] N. Picot-Clemente,[13] F. Pilo,[34] V. Plyaskin,[10] M. Pohl,[16] V. Poireau,[3] L. Quadrani,[8,9] X. M. Qi,[19] X. Qin,[10] Z. Y. Qu,[43,e] T. Räihä,[1] P. G. Rancoita,[29] D. Rapin,[16] J. S. Ricol,[17] S. Rosier-Lees,[3] A. Rozhkov,[10] D. Rozza,[29,30] R. Sagdeev,[12] S. Schael,[1] S. M. Schmidt,[22] A. Schulz von Dratzig,[1] G. Schwering,[1] E. S. Seo,[13] B. S. Shan,[4] J. Y. Shi,[31] T. Siedenburg,[1] J. W. Song,[40] M. Tacconi,[29,30] X. W. Tang,[6] Z. C. Tang,[6] D. Tescaro,[24] J. Tian,[32,33] Samuel C. C. Ting,[10,15] S. M. Ting,[10] N. Tomassetti,[32,33] J. Torsti,[44] T. Urban,[21] V. Vagelli,[32,33] E. Valente,[37,38] E. Valtonen,[44] M. Vázquez Acosta,[24] M. Vecchi,[39,18] M. Velasco,[27] J. P. Vialle,[3] L. Q. Wang,[40] N. H. Wang,[40] Q. L. Wang,[5] X. Wang,[10] X. Q. Wang,[6,7] Z. X. Wang,[19] C. C. Wei,[43,f] J. Wei,[16] Z. L. Weng,[10] K. Whitman,[20] H. Wu,[31] R. Q. Xiong,[31] W. Xu,[10] Q. Yan,[10] M. Yang,[6] Y. Yang,[41] H. Yi,[31] Y. J. Yu,[5] Z. Q. Yu,[6] M. Zannoni,[29,30] S. Zeissler,[23] C. Zhang,[6] F. Zhang,[6] J. Zhang,[10,c] J. H. Zhang,[31] S. W. Zhang,[6,7] Z. Zhang,[10] Z. M. Zheng,[4] H. L. Zhuang,[6] V. Zhukov,[1] A. Zichichi,[8,9] N. Zimmermann,[1] and P. Zuccon[10,35,36]

(AMS Collaboration)

[1]*I. Physics Institute and JARA-FAME, RWTH Aachen University, D–52056 Aachen, Germany*
[2]*Department of Physics, Middle East Technical University (METU), 06800 Ankara, Turkey*
[3]*Laboratoire d'Annecy de Physique des Particules (LAPP), CNRS/IN2P3, Université Grenoble–Alpes, Université Savoie Mont Blanc, F–74000 Annecy, France*
[4]*Beihang University (BUAA), Beijing 100191, China*
[5]*Institute of Electrical Engineering (IEE), Chinese Academy of Sciences, Beijing 100190, China*
[6]*Institute of High Energy Physics (IHEP), Chinese Academy of Sciences, Beijing 100049, China*
[7]*University of Chinese Academy of Sciences (UCAS), Beijing 100049, China*
[8]*INFN Sezione di Bologna, I–40126 Bologna, Italy*
[9]*Università di Bologna, I–40126 Bologna, Italy*
[10]*Massachusetts Institute of Technology (MIT), Cambridge, Massachusetts 02139, USA*
[11]*National Central University (NCU), Chung–Li, Tao Yuan 32054, Taiwan*
[12]*East-West Center for Space Science, University of Maryland, College Park, Maryland 20742, USA*
[13]*IPST, University of Maryland, College Park, Maryland 20742, USA*
[14]*CNR–IROE, I-50125 Firenze, Italy*
[15]*European Organization for Nuclear Research (CERN), CH-1211 Geneva 23, Switzerland*

[16]DPNC, Université de Genève, CH-1211 Genève 4, Switzerland
[17]Laboratoire de Physique Subatomique et de Cosmologie (LPSC), CNRS/IN2P3 and Université Grenoble-Alpes, F–38026 Grenoble, France
[18]KVI—Center for Advanced Radiation Technology, University of Groningen, NL–9700 AB Groningen, Netherlands
[19]Sun Yat–Sen University (SYSU), Guangzhou 510275, China
[20]Physics and Astronomy Department, University of Hawaii, Honolulu, Hawaii 96822, USA
[21]National Aeronautics and Space Administration Johnson Space Center (JSC), Jacobs Engineering, and Business Integra, Houston, Texas 77058, USA
[22]Jülich Supercomputing Centre and JARA-FAME, Research Centre Jülich, D–52425 Jülich, Germany
[23]Institut für Experimentelle Teilchenphysik, Karlsruhe Institute of Technology (KIT), D–76131 Karlsruhe, Germany
[24]Instituto de Astrofísica de Canarias (IAC), E–38205 La Laguna, and Departamento de Astrofísica, Universidad de La Laguna, E–38206 La Laguna, Tenerife, Spain
[25]Laboratório de Instrumentação e Física Experimental de Partículas (LIP), P–1000 Lisboa, Portugal
[26]National Chung–Shan Institute of Science and Technology (NCSIST), Longtan, Tao Yuan 32546, Taiwan
[27]Centro de Investigaciones Energéticas, Medioambientales y Tecnológicas (CIEMAT), E–28040 Madrid, Spain
[28]Instituto de Física, Universidad Nacional Autónoma de México (UNAM), México, D. F., 01000 Mexico
[29]INFN Sezione di Milano–Bicocca, I–20126 Milano, Italy
[30]Università di Milano–Bicocca, I–20126 Milano, Italy
[31]Southeast University (SEU), Nanjing 210096, China
[32]INFN Sezione di Perugia, I–06100 Perugia, Italy
[33]Università di Perugia, I–06100 Perugia, Italy
[34]INFN Sezione di Pisa, I–56100 Pisa, Italy
[35]INFN TIFPA, I–38123 Povo, Trento, Italy
[36]Università di Trento, I–38123 Povo, Trento, Italy
[37]INFN Sezione di Roma 1, I–00185 Roma, Italy
[38]Università di Roma La Sapienza, I–00185 Roma, Italy
[39]Instituto de Física de São Carlos, Universidade de São Paulo, CP 369, 13560-970, São Carlos, São Paulo, SP, Brazil
[40]Shandong University (SDU), Jinan, Shandong 250100, China
[41]National Cheng Kung University, Tainan 70101, Taiwan
[42]Academia Sinica Grid Center (ASGC), Nankang, Taipei 11529, Taiwan
[43]Institute of Physics, Academia Sinica, Nankang, Taipei 11529, Taiwan
[44]Space Research Laboratory, Department of Physics and Astronomy, University of Turku, FI–20014 Turku, Finland

(Received 16 April 2018; revised manuscript received 6 June 2018; published 31 July 2018)

A precision measurement of the nitrogen flux with rigidity (momentum per unit charge) from 2.2 GV to 3.3 TV based on 2.2×10^6 events is presented. The detailed rigidity dependence of the nitrogen flux spectral index is presented for the first time. The spectral index rapidly hardens at high rigidities and becomes identical to the spectral indices of primary He, C, and O cosmic rays above ~700 GV. We observed that the nitrogen flux Φ_N can be presented as the sum of its primary component Φ_N^P and secondary component Φ_N^S, $\Phi_N = \Phi_N^P + \Phi_N^S$, and we found Φ_N is well described by the weighted sum of the oxygen flux Φ_O (primary cosmic rays) and the boron flux Φ_B (secondary cosmic rays), with $\Phi_N^P = (0.090 \pm 0.002) \times \Phi_O$ and $\Phi_N^S = (0.62 \pm 0.02) \times \Phi_B$ over the entire rigidity range. This corresponds to a change of the contribution of the secondary cosmic ray component in the nitrogen flux from 70% at a few GV to < 30% above 1 TV.

DOI: 10.1103/PhysRevLett.121.051103

Nitrogen nuclei in cosmic rays are thought to be produced both in astrophysical sources, mostly via the CNO cycle [1,2], and by the collisions of heavier nuclei with the interstellar medium [3]. Therefore the nitrogen flux Φ_N is expected to contain both primary Φ_N^P and secondary Φ_N^S components. Precise knowledge of the primary component of cosmic nitrogen provides important insights into the details of nitrogen production in astrophysical sources, while precise knowledge of the secondary component of the cosmic nitrogen provides insights into the details of propagation processes of cosmic rays in the Galaxy. Over the last 50 years, few experiments have measured the nitrogen flux [4–7].

Typically, these measurements have errors larger than 40%–50% above 100 GV.

Precision measurements of the primary He, C, and O cosmic ray fluxes and of the secondary Li, Be, and B cosmic ray fluxes by the Alpha Magnetic Spectrometer (AMS) have been reported [8,9] with typical errors of 2%–4% at 100 GV.

To determine the primary and secondary components in the nitrogen flux, we have chosen the rigidity dependence of the oxygen flux as characteristic of primary fluxes and the rigidity dependence of the boron flux as characteristic of secondary fluxes. The secondary component of the oxygen flux is the lowest (a few percent [10,11]) among He, C, and O. The boron flux has no primary contribution and is mostly produced from the interactions of primary cosmic rays C and O with interstellar matter.

In this Letter we report the precision measurement of the nitrogen flux in cosmic rays in the rigidity range from 2.2 GV to 3.3 TV based on data collected by the AMS during the first five years (May 19, 2011 to May 26, 2016) of operation aboard the International Space Station (ISS). The total flux error is 4% at 100 GV.

Detector.—The layout and description of the AMS detector are presented in Ref. [12]. The key elements used in this measurement are the permanent magnet [13], the silicon tracker [14], and the four planes of time of flight (TOF) scintillation counters [15]. Further information on the layout and the performance of the silicon tracker and the TOF is included in Refs. [16,17]. AMS also contains a transition radiation detector (TRD), a ring imaging Čerenkov detector, an electromagnetic calorimeter, and an array of 16 anticoincidence counters.

Nitrogen nuclei traversing AMS were triggered as described in Ref. [18]. The trigger efficiency has been measured to be $> 98\%$ over the entire rigidity range.

Monte Carlo (MC) simulated events were produced using a dedicated program developed by the collaboration based on the GEANT-4.10.1 package [19]. The program simulates electromagnetic and hadronic interactions of particles in the material of AMS and generates detector responses. The Glauber-Gribov model [19], tuned to reproduce the AMS helium data, see supplemental figures SM 1(a),1(b) in Ref. [18], was used for the description of the nuclei inelastic cross sections.

Event selection.—In the first five years AMS has collected 8.5×10^{10} cosmic ray events. The collection time used in this analysis includes only those seconds during which the detector was in normal operating conditions and, in addition, AMS was pointing within 40° of the local zenith and the ISS was outside of the South Atlantic Anomaly. Because of the geomagnetic field, this collection time increases with rigidity, becoming constant at 1.23×10^8 seconds above 30 GV.

Nitrogen events are required to be downward-going and to have a reconstructed track in the inner tracker which passes through $L1$. In the highest rigidity region, $R \geq 1.3$ TV, the track is also required to pass through $L9$. Track fitting quality criteria such as a $\chi^2/\text{d.o.f.} < 10$ in the bending coordinate are applied, similar to Refs. [18,20,21].

The measured rigidity is required to be greater than a factor of 1.2 times the maximum geomagnetic cutoff within the AMS field of view. The cutoff was calculated by backtracing [22] particles from the top of AMS out to 50 Earth's radii using the most recent IGRF model [23].

Charge measurements on $L1$, the upper TOF, the inner tracker, the lower TOF, and, for $R > 1.3$ TV, $L9$ are all required to be compatible with charge $Z = 7$ as shown in Fig. 1 of the Supplemental Material [16] for the inner tracker and in Fig. 2 of the Supplemental Material [16] for the upper TOF for different rigidity ranges. With this selection, the charge confusion from noninteracting nuclei

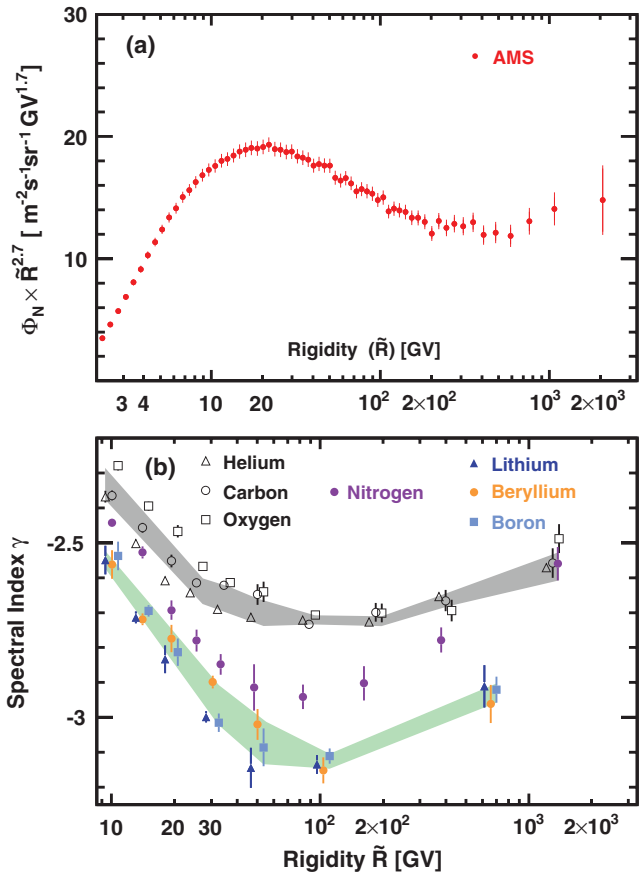

FIG. 1. (a) The AMS nitrogen flux Φ_N [16] multiplied by $\tilde{R}^{2.7}$ with total errors as a function of rigidity. (b) The dependence of the nitrogen spectral index on rigidity together with the rigidity dependence of the spectral indices of primary He, C, and O cosmic rays and secondary Li, Be, and B cosmic rays. For clarity, the horizontal positions of the Li and B data points and He and O data points are displaced with respect to the Be and C data points, respectively. The shaded regions are to guide the eye. As seen, the nitrogen spectral index is situated between the primary and secondary cosmic ray spectral indices, hardens rapidly with rigidity above ~100 GV and becomes identical to the spectral indices of the primary cosmic rays above ~700 GV.

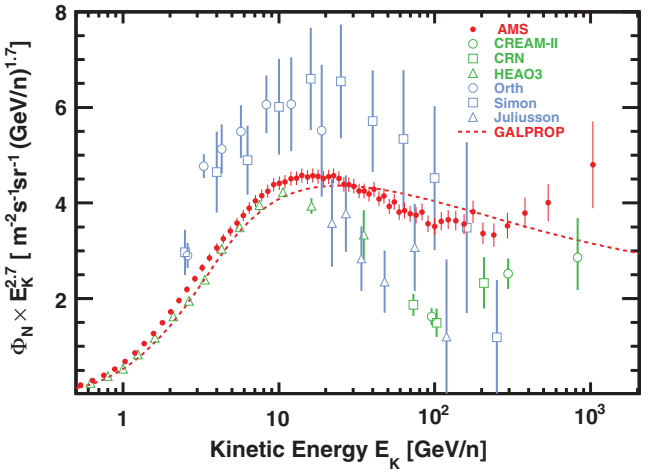

FIG. 2. The AMS nitrogen flux Φ_N as a function of kinetic energy per nucleon E_K multiplied by $E_K^{2.7}$ together with earlier measurements [4–7] and with the predictions of cosmic ray propagation model GALPROP [10] (dashed red curve).

is negligible ($< 0.1\%$) over the whole rigidity range. This selection yields overall purities of 90%–95% depending on rigidity for nitrogen nuclei. The impurities have two sources. First, a residual background to nitrogen events results from the interactions of heavy nuclei such as O, F, and Ne in the material between $L1$ and $L2$ (the TRD and upper TOF). It has been evaluated by fitting the charge distribution from $L1$ of events selected as nitrogen by the inner tracker with charge distribution templates of N, O, F, and Ne. Then cuts are applied on the $L1$ charge as shown in Fig. 3 the Supplemental Material [16]. The charge distribution templates are obtained using $L2$. These templates contain only noninteracting events by requiring that $L1$ and $L3$–$L8$ measure the same charge value. This residual background is $< 5\%$ over the entire rigidity range. Second, the background from O, F, and Ne interacting in materials above $L1$ (thin support structures made of carbon fiber and aluminum honeycomb) has been estimated from simulation using MC samples generated according to AMS flux measurements [8,16,24]. This background is $< 3\%$ below 200 GV and increases up to 6% at 3.3 TV. The simulation of nuclear interactions has been validated using data as shown in Fig. 4 of the Supplemental Material [16].

The overall uncertainty due to the total background subtraction is $< 1.5\%$ over the entire rigidity range. After background subtraction, we obtain 2.2×10^6 nitrogen nuclei.

Data analysis.—The isotropic flux Φ_i in the ith rigidity bin $(R_i, R_i + \Delta R_i)$ is given by

$$\Phi_i = \frac{N_i}{A_i \epsilon_i T_i \Delta R_i}, \tag{1}$$

where N_i is the number of events corrected for bin-to-bin migration, A_i is the effective acceptance, ϵ_i is the trigger efficiency, and T_i is the collection time. In this Letter the nitrogen flux was measured in 66 bins from 2.2 GV to 3.3 TV with bin widths chosen according to the rigidity resolution. Except for the first bin, the bin widths are identical with the bins used in the AMS publication on secondary cosmic rays [9].

The bin-to-bin migration of events was corrected using the unfolding procedure described in Ref. [20]. These

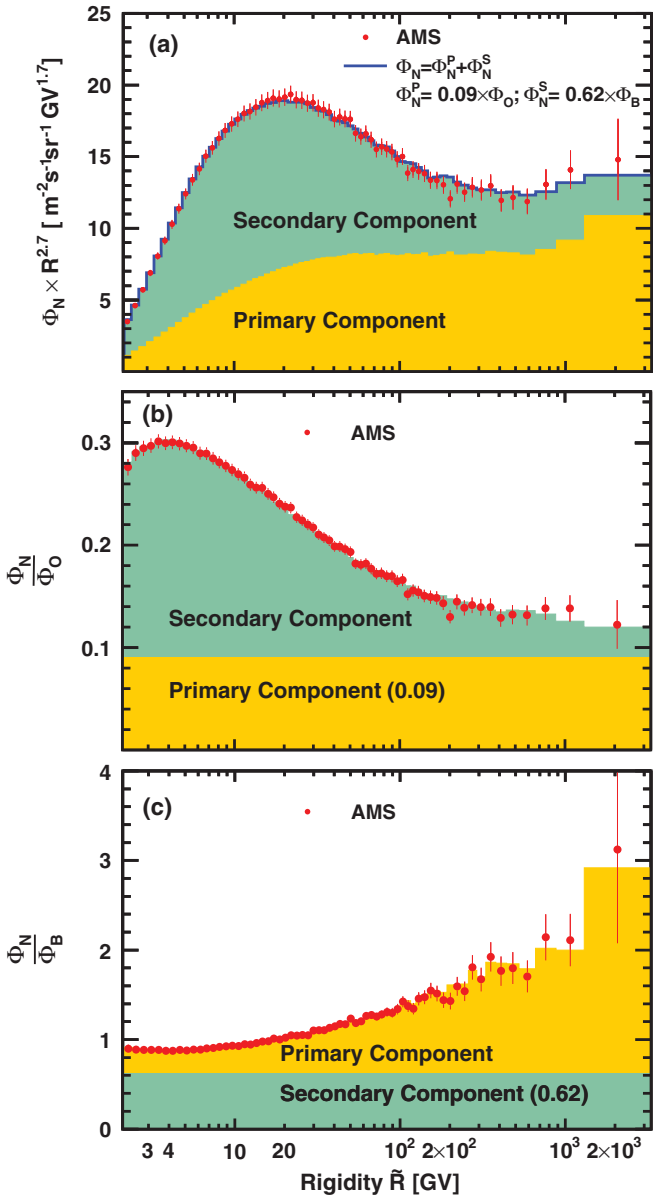

FIG. 3. (a) The AMS nitrogen flux Φ_N fit to the weighted sum of the oxygen flux Φ_O and the boron flux Φ_B over the entire rigidity range. (b) The AMS (Φ_N/Φ_O) ratio as a function of rigidity. (c) The AMS (Φ_N/Φ_B) ratio as a function of rigidity. The contributions of the primary and secondary components are indicated by the shading (yellow and green, respectively). As seen from (b) and (c), the contribution of the secondary component in the nitrogen flux decreases, and the contribution of the primary component correspondingly increases, with rigidity.

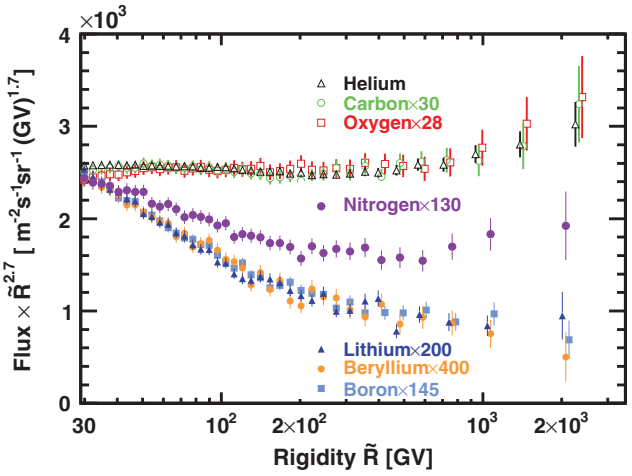

FIG. 4. Comparison of the AMS measurements of the primary cosmic ray fluxes [8] and the secondary cosmic rays fluxes [9] with the nitrogen flux [16] multiplied by $\tilde{R}^{2.7}$ with their total errors as functions of rigidity above 30 GV. For display purposes only, the C, O, Li, Be, B, and N fluxes were rescaled as indicated. For clarity, the horizontal positions of the He, O, Li, and B data points above 400 GV are displaced. As seen, the three secondary fluxes have identical rigidity dependence above 30 GV as do the three primary fluxes above 60 GV, but they are different from each other. The rigidity dependence of the nitrogen flux is distinctly different from the dependence of both the primary fluxes and the dependence of the secondary fluxes.

corrections, $(N_i - \aleph_i)/\aleph_i$, where $\aleph_i$ is the number of observed events in bin i, are $+15\%$ at 3 GV, $+7\%$ at 5 GV, -5% at 200 GV, and -6% at 3.3 TV.

Extensive studies were made of the systematic errors. These errors include the uncertainties in the background estimations discussed above, the trigger efficiency, the geomagnetic cutoff factor, the acceptance calculation, the rigidity resolution function, and the absolute rigidity scale. The systematic error on the flux associated with the trigger efficiency measurement is $< 0.7\%$ over the entire rigidity range. The geomagnetic cutoff factor was varied from 1.0 to 1.4, resulting in a negligible systematic uncertainty ($< 0.1\%$) in the rigidity range below 30 GV.

The effective acceptances A_i were calculated using MC simulation and corrected for small differences between the data and simulated events related to (a) event reconstruction and selection, namely, in the efficiency of velocity determination, track finding, charge determination, and tracker quality cuts and (b) the details of inelastic interactions of nitrogen nuclei in the AMS materials. The total corrections to the effective acceptance from the differences between the data and the MC simulation were found to be $< 3\%$, up to 500 GV and $< 5\%$ at 3.3 TV. The systematic error on the flux associated with the reconstruction and selection is $< 1\%$ over the entire rigidity range. The material traversed by nuclei between $L1$ and $L9$ is composed primarily of carbon and aluminum [18]. The systematic error on the nitrogen flux due to uncertainties of inelastic cross sections for N + C and N + O was evaluated in a similar way as in Ref. [8] and discussed in detail in the data analysis section of the Supplemental Material of Ref. [16]. It was found to be $< 3\%$ up to 100 GV and 4% at 3 TV.

The rigidity resolution function $\Delta(1/R)$ for nitrogen has a pronounced Gaussian core characterized by width σ and non-Gaussian tails more than 2.5σ away from the center [18]. The resolution function has been verified with the procedures described in detail in Ref. [21]. As an example, Fig. 6 of the Supplemental Material of Ref. [16] shows that the measured tracker bending coordinate resolution of 5.5 μm is in good agreement with the simulation. This yields the MDR of 3.5 TV with 5% uncertainty and provides the uncertainties of 10% on the amplitudes of the non-Gaussian tails. The systematic error on the flux due to the rigidity resolution function was obtained by repeating the unfolding procedure while varying the width of the Gaussian core of the resolution function by 5% and by independently varying the amplitudes of the non-Gaussian tails by 10%. The resulting systematic error on the flux is less than 1% below 150 GV and 3% at 3.3 TV.

There are two contributions to the systematic uncertainty on the rigidity scale discussed in detail in Refs. [8,20]. The first is due to residual tracker misalignment. The second contribution arises from the magnetic field map measurement and magnetic field temperature corrections. The error on the flux due to this uncertainty is $< 0.6\%$ up to 100 GV and 5% in the last bin, 1.3–3.3 TV.

Much effort has been spent in understanding the systematic errors [18,20,21]. As an example, Fig. 7 of the Supplemental Material [16] shows the ratio of two measurements of the nitrogen flux from 2.2 GV to 1.3 TV, one performed using events passing through $L1$ to $L8$ and the other using events passing through $L1$ to $L9$. The good agreement between the measurements verifies the systematic errors on unfolding, due to the difference in the resolution functions, and the systematic errors on acceptance, due to the difference in geometric factor and the amount of material traversed.

Most importantly, several independent analyses were performed on the same data sample by different study groups. The results of those analyses are consistent with this Letter.

Results.—The measured nitrogen flux including statistical and systematic errors is reported in Table I of the Supplemental Material [16] as a function of the rigidity at the top of the AMS detector. Figure 1(a) shows the nitrogen flux as a function of rigidity with the total errors, the quadratic sum of statistical and systematic errors. In this and the subsequent figures, the points are placed along the abscissa at $\tilde{R}$ calculated for a flux $\propto R^{-2.7}$ [25].

To examine the rigidity dependence of the flux, the detailed variation of the flux spectral index with rigidity was calculated in a model independent way from

$$\gamma = d[\log(\Phi)]/d[\log(R)], \tag{2}$$

over nonoverlapping rigidity intervals above 8.48 GV with a variable width to have sufficient sensitivity to determine γ. The results are presented in Fig. 1(b) together with the spectral indices of primary cosmic rays He, C, and O [8] and of secondary cosmic rays Li, Be, and B [9]. As seen, the nitrogen spectral index is situated between the primary and secondary cosmic ray spectral indices, hardens rapidly with rigidity above ~100 GV and becomes identical to the spectral indices of He, C, and O above ~700 GV. Figure 2 shows the AMS nitrogen flux as a function of kinetic energy per nucleon E_K together with the results of earlier measurements [4–7] and the prediction of a cosmic ray propagation model, GALPROP [10], which is based on data available before AMS. Data from earlier measurements have been extracted using Ref. [26]. For the AMS measurement $E_K = (\sqrt{Z^2\tilde{R}^2 + M^2} - M)/A$ where Z, M, and A are the nitrogen charge, mass, and atomic mass number, respectively. For comparison with other measurements the atomic mass number of 14.5 was used.

To examine the difference in the rigidity dependence of the nitrogen flux with respect to the fluxes of primary cosmic rays, the nitrogen to oxygen flux ratio N/O was computed using the data in Table I of the Supplemental Material [16] and the data from Ref. [8] and is reported in Table II of the Supplemental Material [16] as a function of rigidity with its statistical and systematic errors. To provide a comparison with previous measurements, the N/O ratio as a function of E_K was computed using the procedure described in Ref. [21] and shown in Fig. 8(a) of the Supplemental Material [16] with total errors as a function of E_K together with earlier measurements [4–7,27,28].

To examine the rigidity dependence of the nitrogen flux with respect to secondary cosmic rays, the nitrogen to boron flux ratio N/B was computed using data in Table I of the Supplemental Material [16] and data from Ref. [9] and is reported in Table III of the Supplemental Material [16] with its statistical and systematic errors as a function of rigidity. Figure 8(b) of the Supplemental Material [16] shows the AMS N/B ratio with total errors as a function of E_K together with the results of earlier measurements [4–6].

To obtain the fractions of the primary $\Phi_{\rm N}^P$ and secondary $\Phi_{\rm N}^S$ components in the nitrogen flux $\Phi_{\rm N} = \Phi_{\rm N}^P + \Phi_{\rm N}^S$, a fit of $\Phi_{\rm N}$ to the weighted sum of a characteristic primary cosmic ray flux, namely, oxygen $\Phi_{\rm O}$ [8], and of a characteristic secondary cosmic ray flux, namely, boron $\Phi_{\rm B}$ [9], was performed over the entire rigidity range, as shown in Fig. 3(a). The fit yields $\Phi_{\rm N}^P = (0.090 \pm 0.002) \times \Phi_{\rm O}$ and $\Phi_{\rm N}^S = (0.62 \pm 0.02) \times \Phi_{\rm B}$ with a $\chi^2/\text{d.o.f.} = 51/64$. Figures 3(b) and 3(c) illustrate the result of this fit in the N/O and N/B ratios, respectively. Figure 9 of the Supplemental Material [16] shows the contributions of the primary and secondary components in the nitrogen flux as functions of rigidity. As seen from Fig. 9 of the Supplemental Material [16], the contribution of the secondary component in the nitrogen flux drops from 70% at a few GV to below 30% above 1 TV. To verify the stability of the result, the fit was repeated in the rigidity range above 60 GV yielding $\Phi_{\rm N} = (0.083 \pm 0.005) \times \Phi_{\rm O} + (0.66 \pm 0.04) \times \Phi_{\rm B}$ with a $\chi^2/\text{d.o.f.} = 18/25$, fully compatible with the results obtained with the fit over the entire rigidity range.

The observation that the nitrogen flux can be fit over a wide rigidity range as the simple linear combination of primary and secondary fluxes is a new and important result, which permits the determination of the N/O abundance ratio at the source without the need to consider the Galactic propagation of cosmic rays.

Finally, Fig. 4 shows the three distinctly different rigidity dependencies above 30 GV of the primary He, C, and O cosmic ray fluxes, the secondary Li, Be, and B fluxes, and the N flux.

In conclusion, a precision measurement of the nitrogen flux in cosmic rays from 2.2 GV to 3.3 TV with detailed studies of the systematic errors has been presented. The flux deviates from a single power law. Its spectral index rapidly hardens at high rigidities starting from ~100 GV and becomes identical to the spectral indices of primary cosmic rays He, C, and O above ~700 GV. Remarkably, the nitrogen flux is well described over the entire rigidity range by the sum of the primary flux $\Phi_{\rm N}^P$ equal to 9% of the oxygen flux [8] and the secondary flux $\Phi_{\rm N}^S$ equal to 62% of the boron flux [9]. This corresponds to a change of the contribution of the secondary component in the nitrogen flux from 70% at a few GV to below 30% above 1 TV.

We thank former NASA Administrator Daniel S. Goldin for his dedication to the legacy of the ISS as a scientific laboratory and his decision for NASA to fly AMS as a DOE payload. We also acknowledge the continuous support of the National Aeronautics and Space Administration (NASA) leadership including Charles Bolden and William H. Gerstenmaier and of the Johnson Space Center (JSC) and Marshall Space Flight Center (MSFC) flight control teams which has allowed AMS to operate optimally on the ISS for seven years. We are grateful for the support of Jim Siegrist and his staff of the DOE including resources from the National Energy Research Scientific Computing Center under Contract No. DE-AC02-05CH11231 and the Argonne Leadership Computing Facility under Contract No. DE-AC02-06CH11357. We also acknowledge the continuous support from MIT and its School of Science, Michael Sipser, Marc Kastner, Ernest Moniz, Richard Milner, and Boleslaw Wyslouch. Research supported by Sáo Paulo Research Foundation (FAPESP) Grants No. 2014/19149-7, No. 2015/50378-5, and No. 2016/10222-9, Brazil; CAS, NSFC, MOST, the provincial governments of Shandong, Jiangsu, Guangdong, and the China Scholarship Council, China; Action H2020 MSCA-IF-2015 under Grant No. 707543-MAtISSE, European Union; the Finnish Funding Agency for Innovation (Tekes) Grants No. 40361/01 and No. 40518/03 and the Academy of Finland Grant

No. 258963, Finland; CNRS/IN2P3, CNES, Enigmass, and the ANR, France; Pascale Ehrenfreund, DLR under Grant No. 50OO1403 and JARA-HPC under Project No. JARA0052, Germany; INFN and ASI under ASI-INFN Agreements No. 2013-002-R.0 and No. 2014-037-R.0, Italy; the Consejo Nacional de Ciencia y Tecnología and UNAM, Mexico; FCT under Grant No. PTDC/FIS/122567/2010, Portugal; CIEMAT, IAC, CDTI, and SEIDI-MINECO under Grants No. ESP2015-71662-C2-(1-P/2-P), No. SEV-2015-0548, No. MDM-2015-0509, and No. RyC-2013-14660, Spain; the Swiss National Science Foundation (SNSF), federal and cantonal authorities, Switzerland; Academia Sinica and the Ministry of Science and Technology (MOST) under Grants No. 103-2112-M-006-018-MY3, No. 105-2112-M-001-003, and No. CDA-105-M06, former Presidents of Academia Sinica Yuan-Tseh Lee and Chi-Huey Wong and former Ministers of MOST Maw-Kuen Wu and Luo-Chuan Lee, Taiwan; the Turkish Atomic Energy Authority under Grants No. 2017TAEK(CERN) A5.H6.F2-15, Turkey; and NSF Grants No. 14255202 and No. 1551980, Wyle Laboratories Grant No. 2014/T72497, and NASA NESSF Grant No. HELIO15F-0005, USA. We gratefully acknowledge the strong support from CERN including Rolf-Dieter Heuer, Fabiola Gianotti, and the CERN IT department including Bernd Panzer-Steindel, and from the European Space Agency including Johann-Dietrich Wörner and Simonetta Di Pippo. We are grateful for important physics discussions with Fiorenza Donato, Jonathan Ellis, Jonathan Feng, Igor Moskalenko, Michael Salamon, Subir Sarkar, Joachim Trümper, Michael S. Turner, and Steven Weinberg.

[a]Also at ASI, I–00133 Roma, Italy.
[b]Also at ASI Space Science Data Center (SSDC), I–00133 Roma, Italy.
[c]Also at Wuhan University, Wuhan 430072, China.
[d]Also at Sun Yat–Sen University (SYSU), Guangzhou 510275, China.
[e]Also at Nankai University, Tianjin 300071, China.
[f]Also at Institute of Theoretial Physics, Chinese Academy of Sciences, Beijing 100190, China.

[1] H. A. Bethe, Phys. Rev. **55**, 434 (1939).
[2] F. Vincenzo, F. Belfiore, R. Maiolino, F. Matteucci, and P. Ventura, Mon. Not. R. Astron. Soc. **458**, 3466 (2016); C. Chiappini, D. Romano, and F. Matteucci, Mon. Not. R. Astron. Soc. **339**, 63 (2003); R. B. C. Henry, M. G. Edmunds, and J. Koppen, Astrophys. J. **541**, 660 (2000).
[3] I. A. Grenier, J. H. Black, and A. W. Strong, Annu. Rev. Astron. Astrophys. **53**, 199 (2015); P. Blasi, Astron. Astrophys. Rev. **21**, 70 (2013); A. W. Strong, I. V. Moskalenko, and V. S. Ptuskin, Annu. Rev. Nucl. Part. Sci. **57**, 285 (2007); A. Castellina and F. Donato, Astrophys. Space Phys. Rev. **24**, 1 (2005).
[4] M. Simon, H. Spiegelhauer, W. K. H. Schmidt, F. Siohan, J. F. Ormes, V. K. Balasubrahmanyan, and J. F. Arens, Astrophys. J. **239**, 712 (1980); C. D. Orth, A. Buffington, G. F. Smoot, and T. S. Mast, Astrophys. J. **226**, 1147 (1978); E. Juliusson, Astrophys. J. **191**, 331 (1974).
[5] J. J. Engelmann *et al.*, Astron. Astrophys. **233**, 96 (1990).
[6] S. Swordy, D. Mueller, P. Meyer, J. L'Heureux, and J. M. Grunsfeld, Astrophys. J. **349**, 625 (1990).
[7] H. S. Ahn *et al.*, Astrophys. J. **707**, 593 (2009).
[8] M. Aguilar *et al.*, Phys. Rev. Lett. **119**, 251101 (2017).
[9] M. Aguilar *et al.*, Phys. Rev. Lett. **120**, 021101 (2018).
[10] We used GALPROP WEBRUN, A. E. Vladimirov, S. W. Digel, G. Jóhannesson, P. F. Michelson, I. V. Moskalenko, P. L. Nolan, E. Orlando, T. A. Porter, and A. W. Strong, Comput. Phys. Commun. **182**, 1156 (2011); with parametrization from R. Trotta, G. Jóhannesson, I. V. Moskalenko, T. A. Porter, R. Ruiz de Austri, A. W. Strong, Astrophys. J. **729**, 106 (2011).
[11] A. Putze, L. Derome, and D. Maurin, Astron. Astrophys. **516**, A66 (2010).
[12] A. Kounine, Int. J. Mod. Phys. E **21**, 1230005 (2012); S. Rosier-Lees, *Proceedings of Astroparticle Physics TEVPA/IDM, Amsterdam, 2014* (unpublished); S. Ting, Nucl. Phys. B, Proc. Suppl. **243–244**, 12 (2013); S.-C. Lee, *Proceedings of the 20th International Conference on Supersymmetry and Unification of Fundamental Interactions (SUSY 2012), Beijing, 2012* (unpublished); M. Aguilar, *Proceedings of the XL International Meeting on Fundamental Physics, Centro de Ciencias de Benasque Pedro Pascual, 2012* (unpublished); S. Schael, *Proceedings of the 10th Symposium on Sources and Detection of Dark Matter and Dark Energy in the Universe, Los Angeles, 2012* (unpublished); B. Bertucci, Proc. Sci., EPS-HEP, (**2011**) 67; M. Incagli, AIP Conf. Proc. **1223**, 43 (2010); R. Battiston, Nucl. Instrum. Methods Phys. Res., Sect. A **588**, 227 (2008).
[13] K. Lübelsmeyer *et al.*, Nucl. Instrum. Methods Phys. Res., Sect. A **654**, 639 (2011).
[14] B. Alpat *et al.*, Nucl. Instrum. Methods Phys. Res., Sect. A **613**, 207 (2010).
[15] V. Bindi *et al.*, Nucl. Instrum. Methods Phys. Res., Sect. A **743**, 22 (2014).
[16] See Supplemental Material at http://link.aps.org/supplemental/10.1103/PhysRevLett.121.051103 for details of the AMS detector and data analysis; for the tabulated nitrogen flux, the nitrogen to oxygen and nitrogen to boron flux ratios as functions of rigidity; and for several figures regarding charge resolution and selection, survival probabilities, tracker residuals, other detailed systematic studies, the N/O and N/B ratios vs E_K compared with earlier measurements, and the composition of Φ_N.
[17] G. Ambrosi, V. Choutko, C. Delgado, A. Oliva, Q. Yan, and Y. Li, Nucl. Instrum. Methods Phys. Res., Sect. A **869C**, 29 (2017).
[18] M. Aguilar *et al.*, Phys. Rev. Lett. **115**, 211101 (2015).
[19] J. Allison *et al.*, Nucl. Instrum. Methods Phys. Res., Sect. A **835**, 186 (2016); S. Agostinelli *et al.*, Nucl. Instrum. Methods Phys. Res., Sect. A **506**, 250 (2003).
[20] M. Aguilar *et al.*, Phys. Rev. Lett. **114**, 171103 (2015).
[21] M. Aguilar *et al.*, Phys. Rev. Lett. **117**, 231102 (2016).
[22] J. Alcaraz *et al.*, Phys. Lett. B **484**, 10 (2000).
[23] C. C. Finlay *et al.*, Geophys. J. Int. **183**, 1216 (2010); E. Thébault *et al.*, Earth Planet Space **67**, 79 (2015).
[24] M. Aguilar *et al.* (AMS Collaboration), Measurement of the Flux of Light Nuclei in Primary Cosmic Rays with the

Alpha Magnetic Spectrometer on the International Space Station (to be published).
[25] G. D. Lafferty and T. R. Wyatt, Nucl. Instrum. Methods Phys. Res., Sect. A **355**, 541 (1995). We have used Eq. (6) with $\tilde{R} \equiv x_{lw}$.
[26] D. Maurin, F. Melot, and R. Taillet, Astron. Astrophys. **569**, A32 (2014).
[27] H. S. Ahn *et al.*, Astropart. Phys. **30**, 133 (2008).
[28] A. D. Panov *et al.*, Bull. Russian Acad. Sci. **73**, 564 (2009).